energies

Article

Influence of High-Speed Train Power Consumption and Arc Fault Resistances on a Novel Ground Fault Location Method for 2 × 25 kV Railway Power Supply Systems

Carlos A. Platero [1,*], Jesús Serrano [1], Máximo López-Toledo [1] and Ricardo Granizo [2]

1 Department of Electrical Engineering, ETS Ingenieros Industriales, Universidad Politécnica de Madrid, C/José Gutierrez Abascal, 2, 28006 Madrid, Spain; jserranoalv@hotmail.com (J.S.); maximo.lopez@upm.es (M.L.-T.)
2 Department of Electrical Engineering, ETS Ingeniería y Diseño Industrial, Universidad Politécnica de Madrid, C/Ronda de Valencia, 3, 28012 Madrid, Spain; ricardo.granizo@upm.es
* Correspondence: carlosantonio.platero@upm.es; Tel.: +34-91-067-69-77; Fax: +34-91-336-30-08

Received: 17 May 2018; Accepted: 15 June 2018; Published: 19 June 2018

Abstract: The 2 × 25 kV power supply system is the most frequently used traction rail system to provide the huge power needed by high-speed trains. However, locating the ground fault in this power supply system is more complicated than in other configurations of electrical railway power supply due to the installation of autotransformers throughout the line section. In previous papers, the authors have described a ground fault location method with an insignificant installation cost. The method and, moreover, the location discriminate between whether the ground fault is located between a positive conductor and ground or a negative conductor and ground. The current of the high-speed train influences the accuracy of the location of the ground fault. An additional factor which influences the location method is the existence of an arc resistance between the positive or negative conductor and ground. In this paper, the influence of high-speed train currents and arc resistances are analysed to evaluate the error in the location method. The major conclusion of the paper is that the location method has an acceptable precision even taking into consideration the high-speed train current and arc resistance. The validation of the method has been performed by laboratory tests and computer simulations with satisfactory results.

Keywords: electrical protection; ground faults; fault location; railways power system; 2 × 25 kV

1. Introduction

High-speed trains are one of the more effective and faster modes of transport between medium and big cities with distances in the range of 600 km.

To supply the high power demand of these trains, a 2 × 25 kV AC power supply system is used, due to the advantages of providing high power with lower currents and fewer traction substations on the line [1].

In a 2 × 25 kV supply system, the power in the line is supplied by some traction substations (TSs). Each substation feeds two sections, one in each direction, and each section is formed by some subsections delimited by autotransformers (ATs). At the end of each section, a final autotransformer (SATS) is installed. The 2 × 25 kV power supply systems have three conductors. The positive conductor (usually named as the catenary) is at 25 kV AC voltage with a positive polarity from ground. The negative voltage conductor (usually named as the feeder) is at 25 kV AC voltage with a negative polarity from ground. Finally, the third conductor is the rail, which is grounded [2]. Figure 1 displays the simplified diagram of a 2 × 25 kV power system section comprising three subsections (A, B, and C), delimited by three autotransformers (ATS 1, ATS 2, and SATS). The current distribution is represented when a train is located in the midpoint of subsection B.

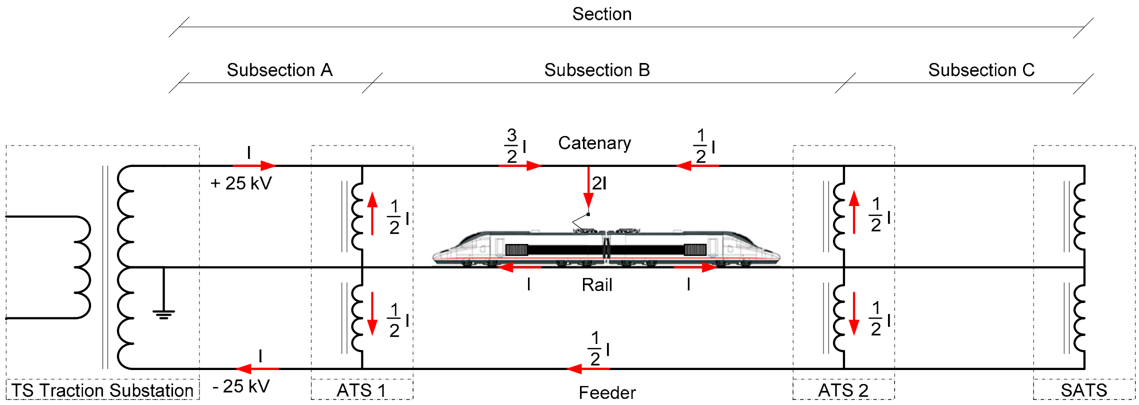

Figure 1. Simplified scheme of a 2 × 25 kV rail power system.

Traction railway power supply systems must be protected by electrical relays, which ensure they will work effectively and reliably. Also, due to the physical configuration (proximity to bushes of the electric line, slipping of the pantograph on the catenary), railway power supply systems have a larger number of ground faults than other electrical installations [3]. It is necessary to detect and locate ground faults in a reliable and fast way in order to repair them as fast as possible without large interruptions of the railway service. However, locating the ground faults in these 2 × 25 kV systems is more difficult than in other AC traction rail systems, which use the impedance method to measure the length from the substation to the ground fault position [4].

The impedance/distance ratio is not linear in a 2 × 25 kV power supply system, so the impedance method cannot be used [5].

There are different methods based on underimpedance relays, which present advantages and disadvantages. Some of them are based on the individualization of the catenary and feeder circuits [6]. Others use numerous underimpedance relays installed in every autotransformer and sectionalizing point [7].

There are methods based on different measurements, such as the current relations of the neutral connection in autotransformers [8,9] or measurements made by fault current sensor installations at the connections between the rail and the air cable of ground return [10]. Other research lines are the progressive wave location method [11,12], the domain frequency location methods [13], and methods which compare models in the time domain with others in the frequency domain [14].

A novel method of identifying the subsection between autotransformers where the ground fault has happened and identifying the faulty conductor was presented in [15]. This identification method, combined with an analysis of the currents in the autotransformers, allowed the location method presented in [16] to be developed.

There are some factors which can produce errors in the ground fault location, such as the fault arc resistance or the train circulation.

In this paper, the influence of high-speed train currents and arc resistances is analysed to evaluate the error in the location method presented in [16].

This article is structured as follows: Section 2 offers a short description of the ground fault location method. Then, Section 3 details the influence of the high-speed train power demand and fault arc resistance in the short-circuit current. Section 4 analyses the computer simulations, and Section 5 analyses the experimental results. Finally, Section 6 presents the contributions of the article.

2. Short Description of the Ground Fault Location Method for 2 × 25 kV Supply Systems

This new ground fault location method for 2 × 25 kV railways power systems is founded on the comparison of the angles between currents and voltages in the autotransformers as well as the module values of these currents when the ground fault happens.

This ground fault location method comprises three steps (Figure 2).

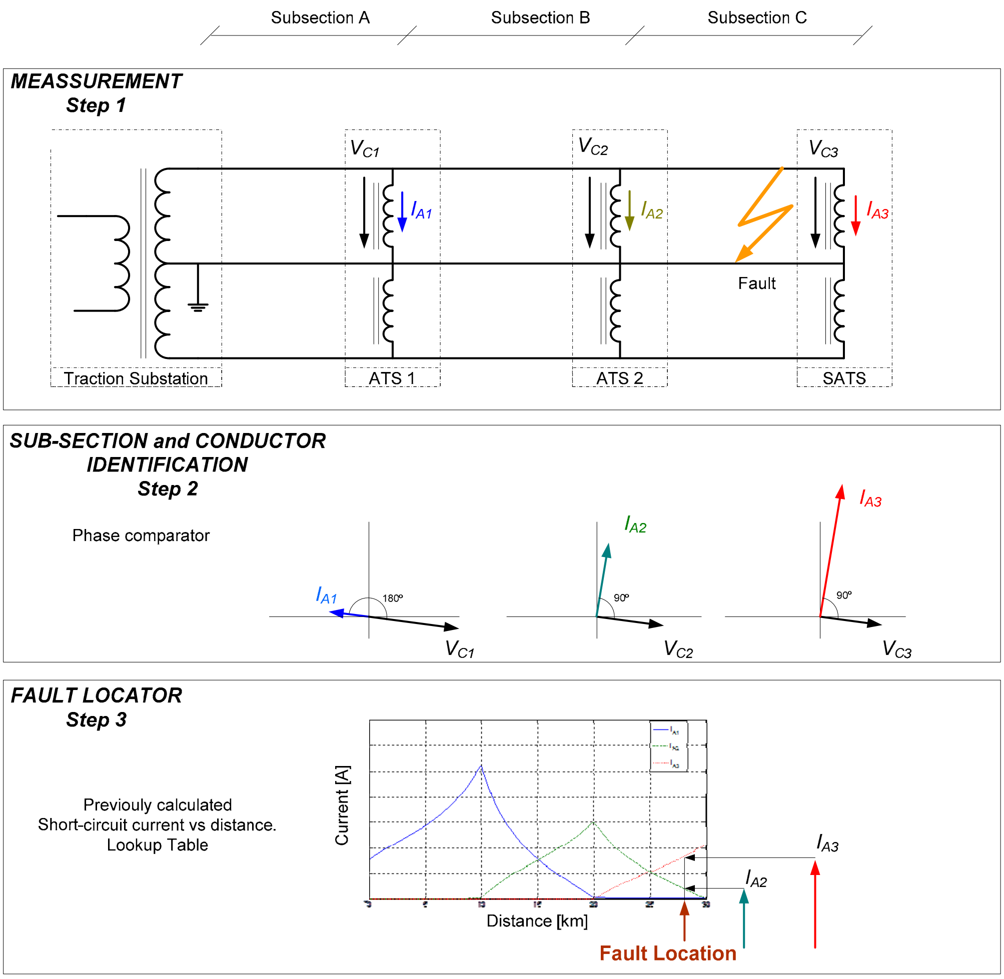

Figure 2. Simplified layout of the location method for 2 × 25 kV rail power system.

2.1. Measurement

If a ground fault occurs, there are overcurrents in the adjacent autotransformers. The autotransformer currents will surpass a certain limit, and the location system is started.

In this first step, it is necessary to record the currents and voltages (V_{C1}, I_{A1}; V_{C2}, I_{A2}; V_{C3}, I_{A3}) in the autotransformers. Also, the phase angle between them should be recorded.

2.2. Subsection and Conductor Identification

Then, the subsection and the conductor where the fault has occurred are recognized by the analysis of the angle between the voltages and currents previously measured in the autotransformers. The complete method is described in [15].

According to [15], when a fault occurs between the rail and catenary or between the rail and feeder, there is an important increase in the current of the windings of the autotransformers adjacent to the ground fault. Moreover, the angles between the currents and voltages change 90° at the autotransformers.

Figure 3 presents, as an example, a diagram of a 2 × 25 kV section with three subsections where a fault between the rail and the catenary has occurred. The angles between I_{A2} and V_{C2} and between I_{A3} and V_{C3} are decreased from close to 180° to near to 90°.

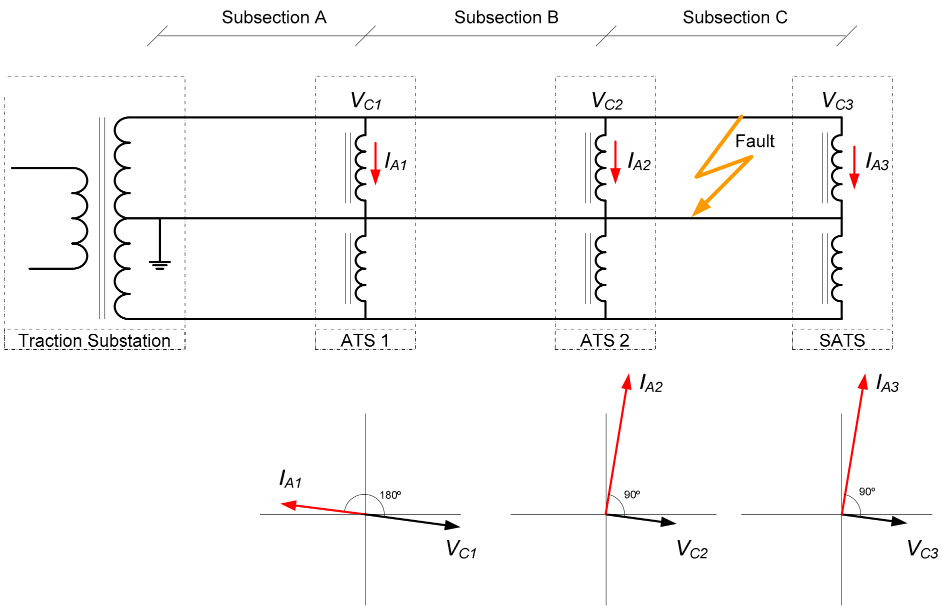

Figure 3. Diagram of a 2 × 25 kV power system with a ground fault in the catenary in subsection C.

2.3. Fault Locator

Finally, the fault locator is founded on a previous calculation of the currents in the autotransformers in case of a ground fault at all positions of a section [16].

The previous calculations should be made considering the particular data of the 2 × 25 kV power system. The values of the autotransformer currents, in the case of a ground fault, must be stored as look-up tables.

The fault is located by comparing the current recorded in the adjacent autotransformers with the values stored in the look-up tables previously. Thereby, the ground fault can be located.

One typical distribution of the autotransformer currents in the case of a ground fault along the section is shown in Figure 4 as an example.

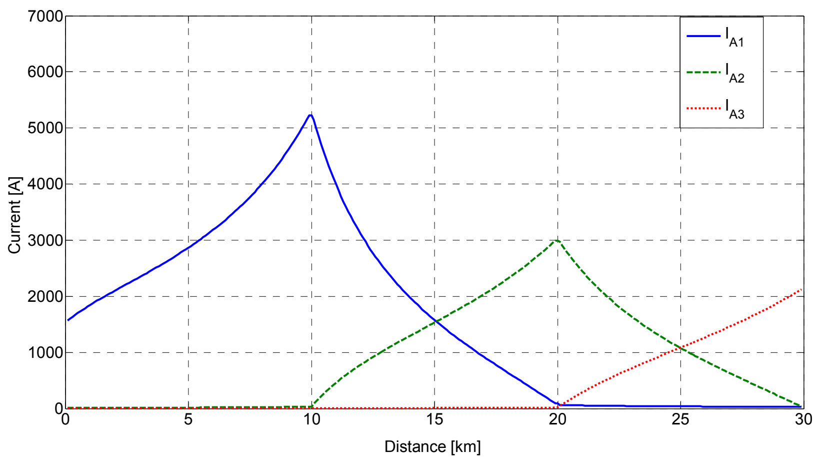

Figure 4. Simulated currents in 2 × 25 kV power system with autotransformers AT1, AT2, and SATS for different fault locations. Fault between rail and catenary.

3. Influence of High-Speed Train Power Demand and Fault Resistances

The aim of this article is to analyse the influence of the train circulation and arc resistance on the new ground fault location method presented in [16].

As the location method is based on a comparison between the calculated and measured currents, the circulation of trains or the arc resistance could produce an error in the location.

Therefore, the influence of these factors on the current modules in these autotransformers as well as on the angles between currents and voltage in the autotransformers when the ground fault occurs will be studied.

3.1. High-Speed Power Consumption in a 2 × 25 kV Railway Power Supply System

To analyse the effect of the train power demand on the accuracy of the location method, a current source has been included in the circuit presented in Figure 3. The maximum power demand considered during the acceleration is 14.63 MW. This is represented by a current (I) of 616 A with a 0.95 power factor. As an example, in the Figure 5, the current source is located in the midpoint of subsection B, but different train locations and different operation points have also been studied.

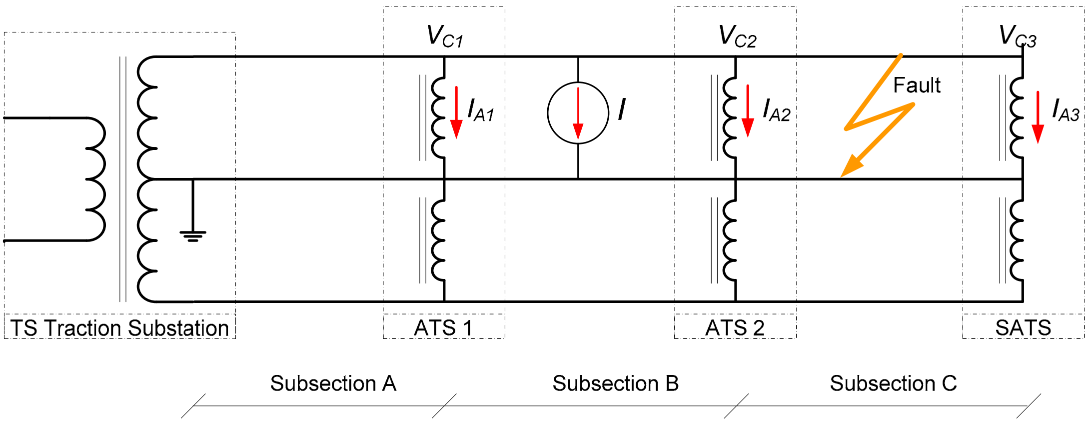

Figure 5. 2 × 25 kV power supply section including a train.

3.2. Fault Resistances in 2 × 25 kV Railway Power Supply Systems

The fault resistance is related to the insulation distance and the fault current. In this paper, it is considered that the ground fault can be produced between the catenary and the sustenance pole or between the feeder and the sustenance pole. The insulation distance (L) between the catenary or feeder and the sustenance post is 400 mm (Figure 6).

According to [17], different models of fault resistance estimation have been developed by Warrington (1), Mason (2), Goda (3), Terzija and Koglin (4), and Blackburn and Domin (5).

Warrington:

$$R = \frac{28707.35\ L}{I^{1.4}} \tag{1}$$

Mason:

$$R = \frac{1804.46\ L}{I} \tag{2}$$

Goda:

$$R = \left[\frac{950}{I} + \frac{5000}{I^2}\right] L \tag{3}$$

Terzija and Koglin:

$$R = \left[\frac{855.30}{I} + \frac{4501.58}{I^2}\right] L \tag{4}$$

Blackburn and Domin:

$$R = \frac{1443.57\, L}{I} \quad (5)$$

where

R Arc resistance (Ω)
L Arc length (m)
I RMS value of the fault current (A)

These expressions have been developed thanks to numerous experimental tests of different current ranges [17]. According to the railway geometry and the fault current levels, Mason's model has been chosen.

The error produced by the arc resistance would be higher for lower values of fault currents. Considering 2500 A as the value of fault current and an arc length of 0.40 m, the fault resistance to be considered is 0.2887 Ω. An arc resistance of 0.29 Ω is therefore considered in the simulation model.

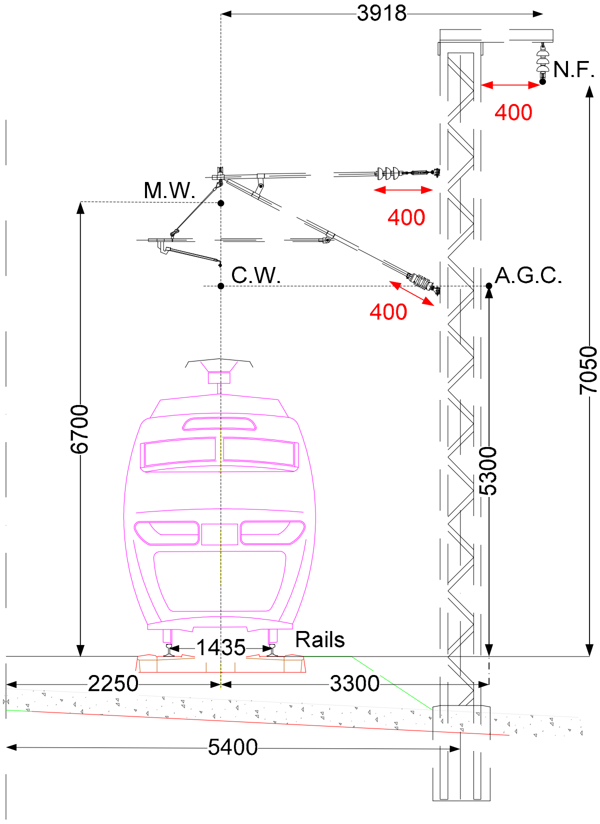

Figure 6. Typical high-speed railway geometry considered for simulation.

4. Simulations

Numerous computer simulations have been performed to analyse the effect of the high-speed train circulation and fault resistance in the ground fault location.

The circuit presented in Figure 7 was programmed in Matlab® (Version 2016b, MathWorks, Inc., Natick, MA, USA). The modified nodal circuit analysis method was used [18]. The circuit was fed from one end by two 25 kV AC sources. A 10-km length was used for the three subsections A, B, and C.

These simulations are described in the next subsections.

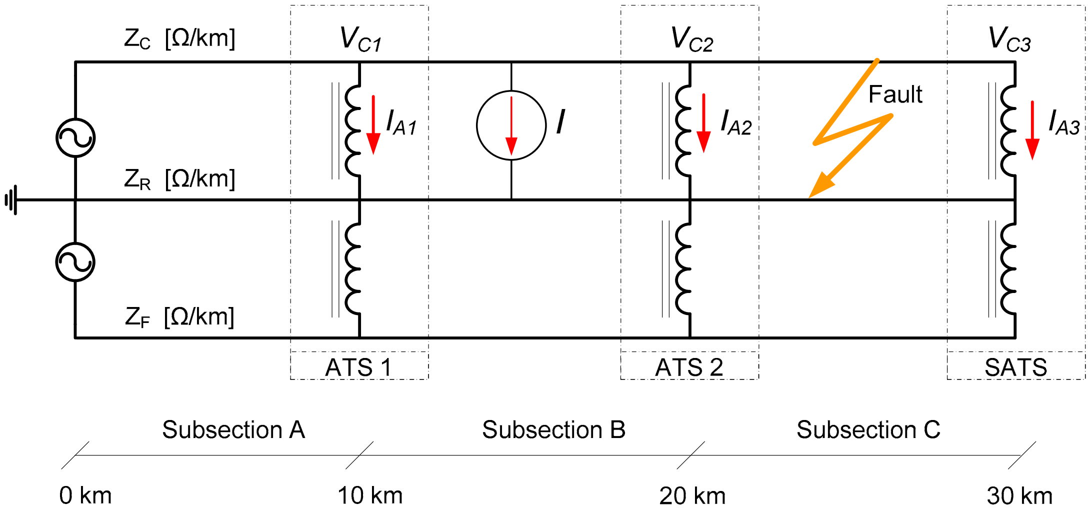

Figure 7. Equivalent circuit of 2 × 25 kV power supply section including a train for simulation.

4.1. *Simulations of the Influence of Train Power Consumption*

In order to simulate the 2 × 25 kV power system in the case of a ground fault with a train circulating in the section, the circuit shown in Figure 7 was employed. Thanks to the simulations, the changes in the phase angle between the currents and voltages in the autotransformers as well as the current modules have been obtained.

As stated before, the current source for simulating a train corresponds to 616 A with a power factor of 0.95. Additional simulations have been included considering one of the trains at one third of the rated power (4.88 MW)

The mutual and self-impedances employed in the simulation are listed in Table 1. These impedances correspond to the catenary and feeder configuration presented in Figure 6.

Employing the circuit shown in Figure 7, different MATLAB® simulations were developed, with short-circuits between the rail and the catenary and between the rail and the feeder. The ground faults were simulated along the three subsections A, B, and C, including the existence of one or two trains in the midpoint of each subsections.

Table 1. Self and mutual impedance of 2 × 25 kV power system.

Conductor		Impedance (Ω/km)	Conductor		Impedance (Ω/km)
Catenary	Z_C	0.1197 + j0.6224	Catenary–feeder	Z_{CF}	0.0480 + j0.3401
Feeder	Z_F	0.1114 + j0.7389	Catenary–rail	Z_{CR}	0.0491 + j0.3222
Rail	Z_R	0.0637 + j0.5209	Feeder–rail	Z_{FR}	0.0488 + j0.2988

4.1.1. Influence of Train Consumption on Current-Voltage Phase in Autotransformer in the Case of a Ground Fault

The phase angles between voltages and currents in the autotransformers ATS 1, ATS 2, and SATS were also analysed from the simulation results. In this section, several examples have been included. Figures 8 and 9 show the angles with a train circulating at the midpoint of the subsection A with faults between catenary and ground and feeder and ground.

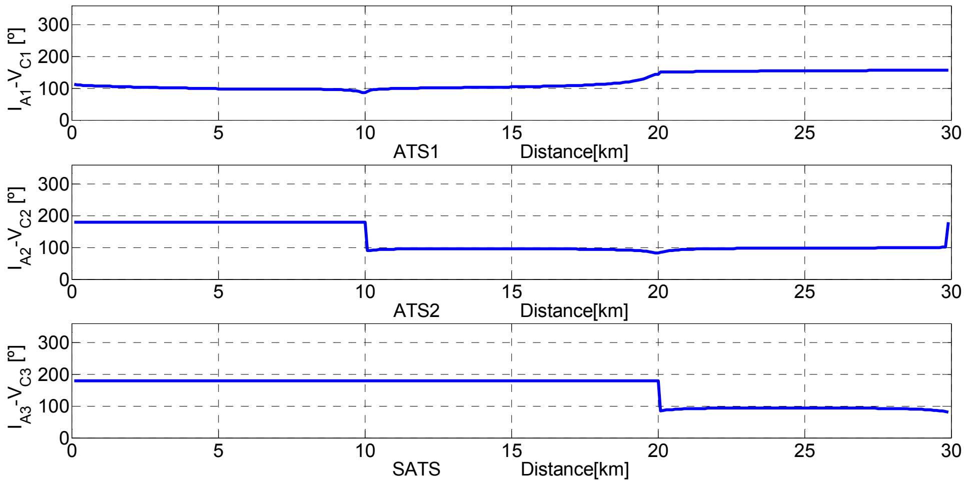

Figure 8. Phase angles between I_A and V_C at different ATSs as a function of the distance from the fault to the substation. Fault considered between catenary and rail with a train at the midpoint of the subsection A.

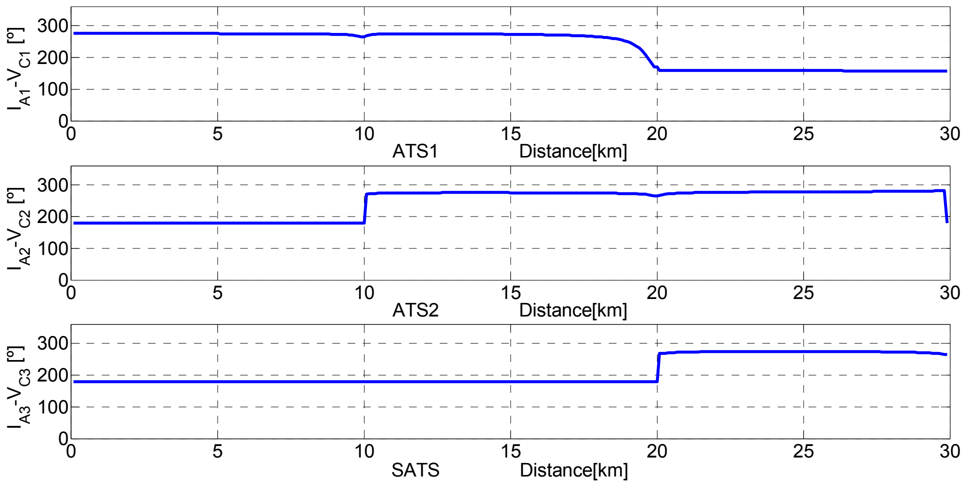

Figure 9. Angles between I_A and V_C as a function of the distance from the fault to the traction substation. Fault between rail and feeder with a train at the midpoint of subsection A.

Additionally, Figures 10 and 11 show the phase angles between current and voltage at the autotransformers with two trains circulating with faults between catenary and ground in the first case and faults between feeder and ground in the second case. In the simulation presented in Figure 10, the trains circulate at the midpoints in subsections A and B, and in the simulations presented in Figure 11, the trains circulate at the midpoints in subsections A and C.

The second step of the ground fault location method is based on the phase shift between voltage and current in the case of a ground fault. According to the simulation results, the influence of the train circulation on the phase angles is very small. Only in the case of a ground fault close to the autotransformers is there a slight difference from the theoretical decrease of 90° when there is a catenary–ground fault or from the theoretical increase of 90° in the case of a feeder–ground fault. These small deviations in the phase angle do not produce the incorrect operation of the directional overcurrent relays because these relays have a phase angle tripping area in the range of ±30°.

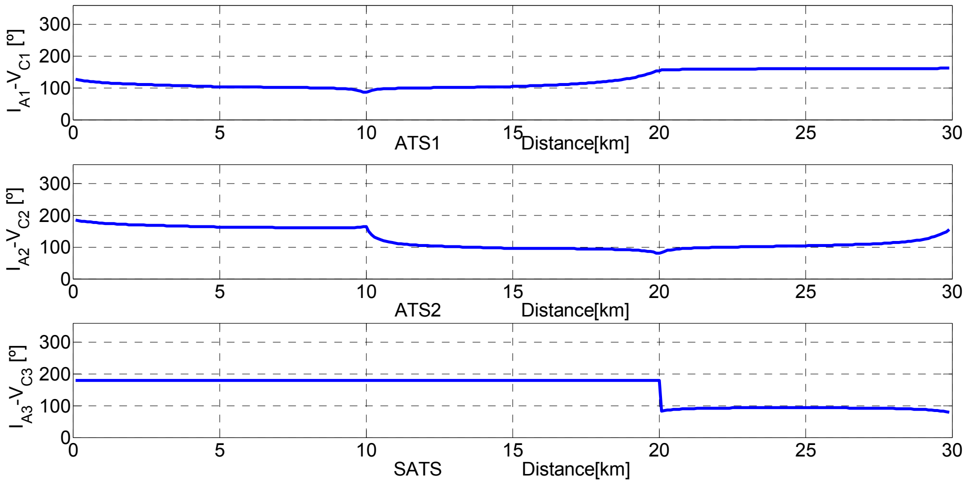

Figure 10. Angles between I_A and V_C as a function of the distance from the fault to the traction substation. Fault between rail and catenary with two trains at the midpoint of subsections A and B, respectively.

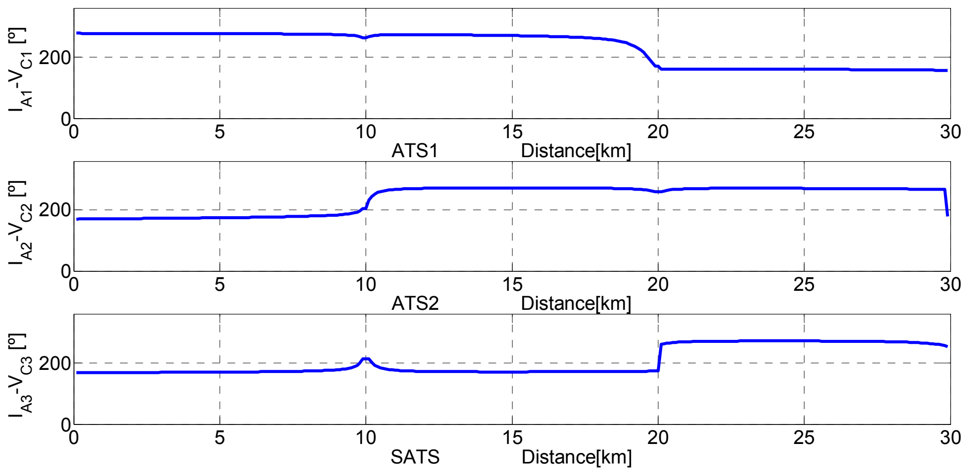

Figure 11. Angles between I_A and V_C as a function of the distance from the fault to the traction substation. Fault considered between rail and feeder with two trains at the midpoint of subsections A and C, respectively.

4.1.2. Influence of Train Consumption on the Autotransformer Currents in the Case of a Ground Fault

This simulation model is similar to that shown in the previous subsection. Numerous simulations have been performed, but only some of them are presented as examples with the train circulation in the case of faults between catenary and ground and between feeder and ground.

In this case, the currents in the autotransformers are represented for ground faults along the section in the case of one train circulating in the subsection C (I_{A1t1}) and two trains circulating in subsections A and B (I_{A1t2}).

The results for ground faults between catenary and ground are presented in Figure 12, where the currents in the case of no trains in the section are also presented. On the other hand, the cases of ground faults between feeder and ground are presented in Figure 13.

According to the results, the influence of train circulation is negligible, as the currents supplied by the autotransformer are similar in all cases.

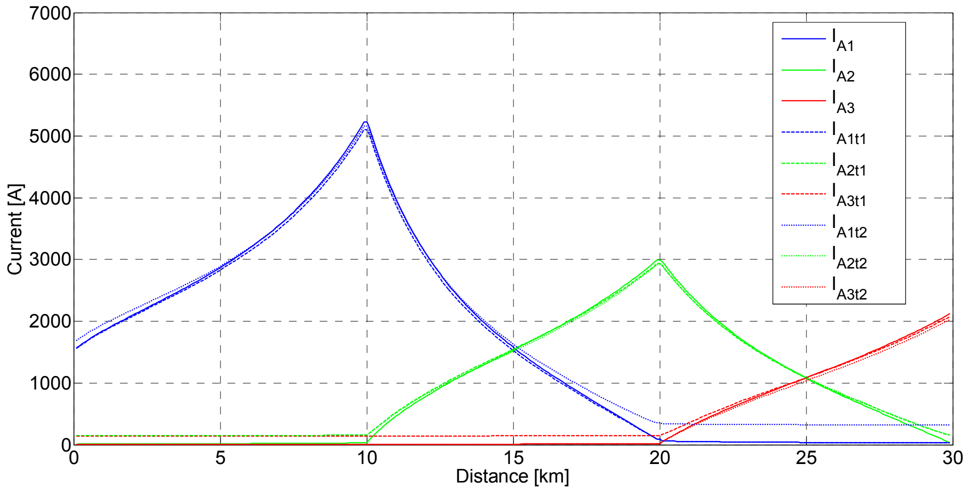

Figure 12. Simulated currents of the autotransformers AT1, AT2, and SATS for different fault locations. Fault between catenary and rail. Cases: (**a**) no trains (I_{Ai}), (**b**) one train at the midpoint of subsection C (I_{Ait1}), and (**c**) two trains at the midpoint of subsections A and B (I_{Ait2}).

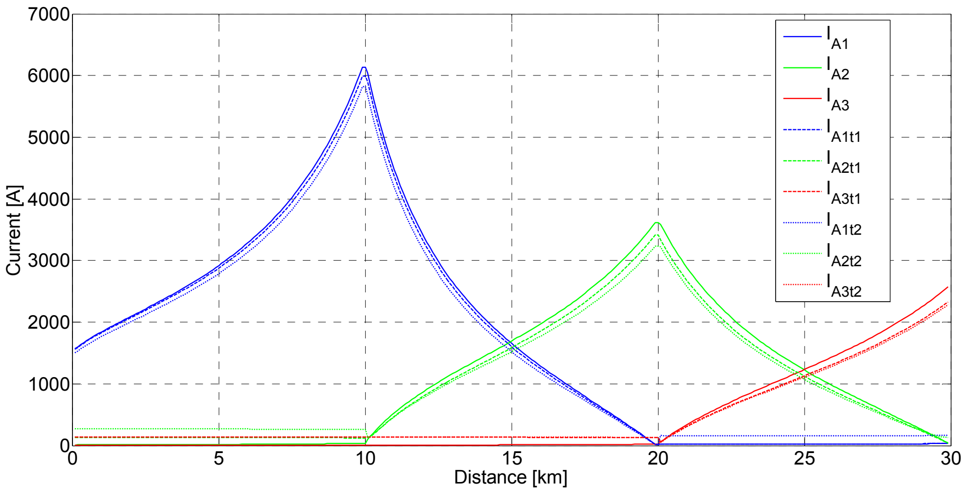

Figure 13. Simulated currents of the autotransformers AT1, AT2, and SATS for different fault locations. Fault between feeder and rail. Cases: (**a**) no trains (I_{Ai}), (**b**) one train at the midpoint of subsection C (I_{Ait1}), and (**c**) two trains at the midpoint of subsections B and C (I_{Ait2}).

During the acceleration of the train, the power consumption is maximal, but in the case of constant-speed operation, the power is considerably reduced. Also considered in the simulations are trains at one third of their maximum power (4.88 MW), representing the constant-speed operation. Ground faults between catenary and rail along the section are presented in Figure 14, representing the case of one train circulating in the midpoint of subsection C (I_{A1t1}) and two trains circulating in subsections A and B (I_{A1t2}), the second one at constant-speed operation. The results are similar to those presented in Figure 12.

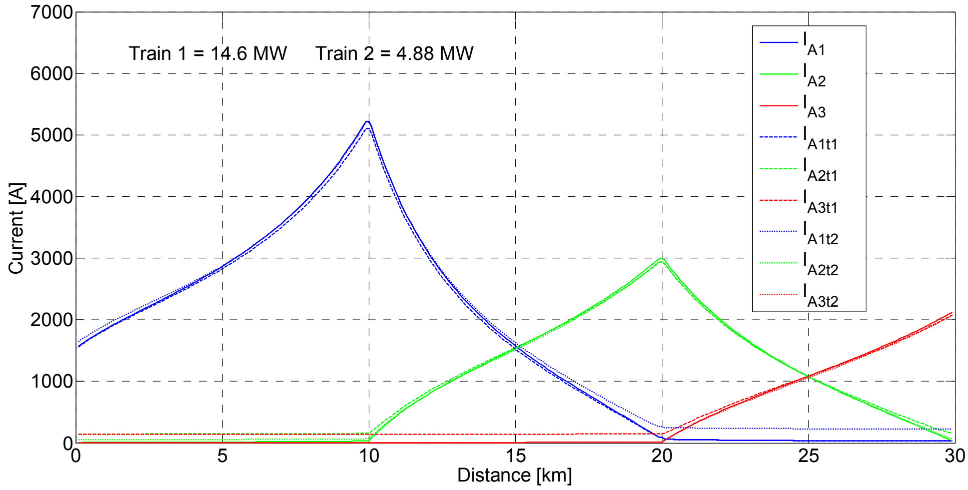

Figure 14. Simulated currents of the autotransformers AT1, AT2, and SATS for different fault locations. Fault between catenary and rail. Cases: (**a**) no trains (I_{Ai}), (**b**) Train 1 at the midpoint of subsection C (I_{Ait1}), and (**c**) Train 1 midpoint of subsection A and Train 2 midpoint of subsection B (I_{Ait2}). Train 1 power 14.6 MW and Train 2 power 4.88 MW.

4.2. Simulations of the Influence of Fault Resistance

In order to study the influence on the angles between the current and the voltage and the current modules in the autotransformers when the ground fault occurs with an arc resistance, numerous simulations have been performed.

The simulations are based on the system presented in Figure 15. In these simulations, a fault resistance (R) of 0.29 Ω has been used, as described in the previous section. Catenary–rail faults and feeder–rail faults were simulated along the section.

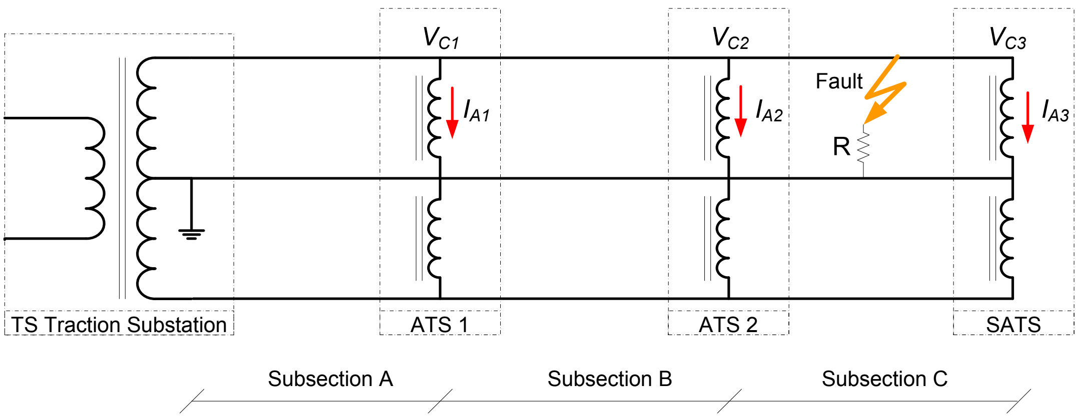

Figure 15. 2 × 25 kV simulation model for ground faults with an arc resistance R.

4.2.1. Influence of Fault Resistance on Current-Voltage Phase in Autotransformer in the Case of a Ground Fault

Figure 16 shows the phase angle between the currents and voltages at the different autotransformers in the case of a catenary–ground fault with an arc resistance of 0.29 Ω.

Additionally, Figure 17 shows the phase angle between current and voltage in the autotransformers in the case of a feeder–ground fault with an arc resistance of 0.29 Ω.

It can be clearly seen that in both cases, the deviations of the angles are small. These small deviations in the phase angle do not produce the incorrect operation of the directional overcurrent relays because these relays have a phase angle tripping range area of ±30°.

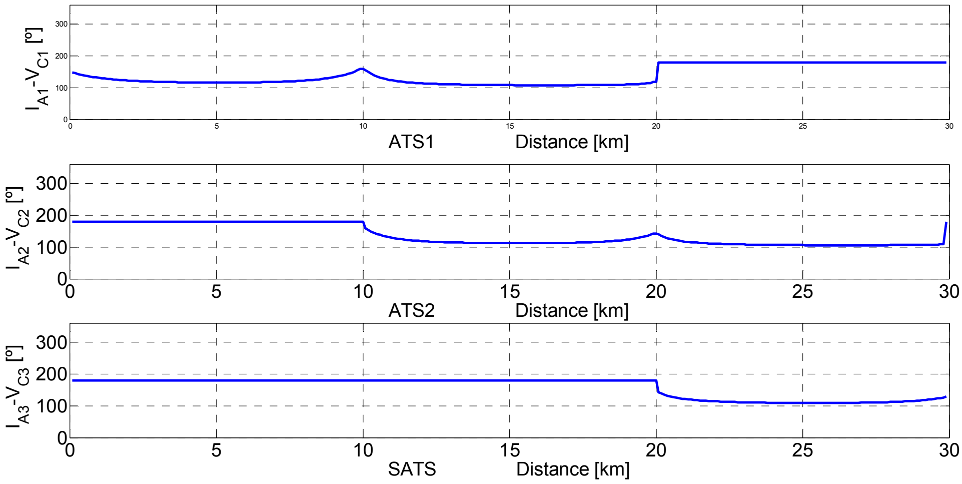

Figure 16. Phase angles between I_A and V_C at different ATSs as a function of the distance from the fault to the substation. Fault between catenary and ground; fault resistance of 0.29 Ω.

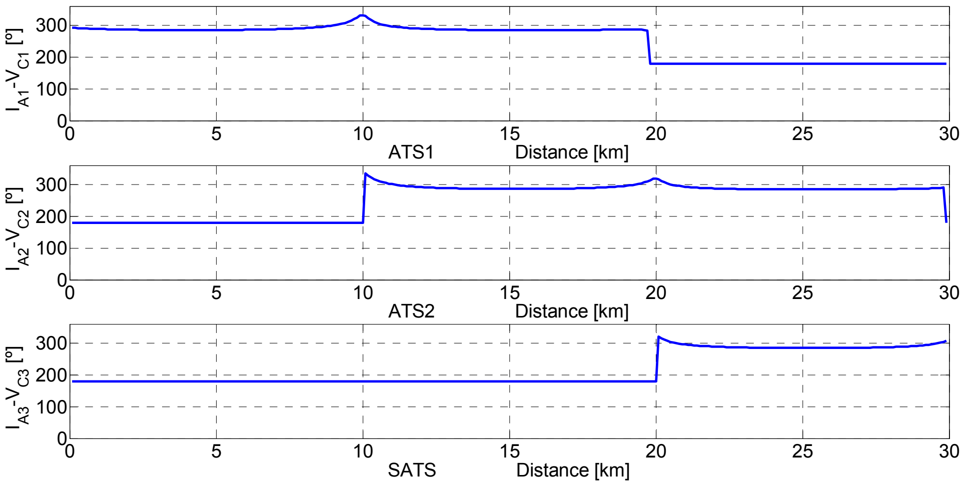

Figure 17. Phase angles between I_A and V_C at different ATSs as a function of the distance from the fault to the substation. Fault considered between feeder and ground; fault resistance of 0.29 Ω.

4.2.2. Influence of Fault Resistance on the Autotransformer Currents in the Case of a Ground Fault

The current modules in the autotransformers when a ground fault happens in the catenary are shown in Figure 18. Two cases are presented: (1) without fault resistance and (2) with an arc resistance of 0.29 Ω.

Additionally, a comparison of the current modules in the autotransformers with feeder ground faults with or without fault resistance are shown in Figure 19.

As shown in Figures 18 and 19, the influence of the fault resistance on the current values in the autotransformers is insignificant. The different between the two cases is less than 1.5% in any case.

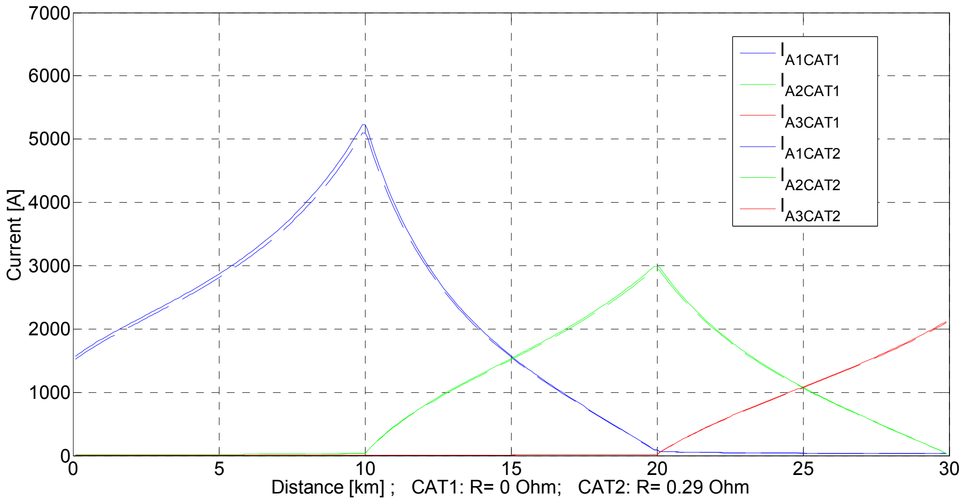

Figure 18. Simulated currents of the autotransformers AT1, AT2, and SATS for different fault locations. Fault between catenary and rail. Cases: (1) CAT1—no fault resistance, (2) CAT2—fault resistance of 0.29 Ω.

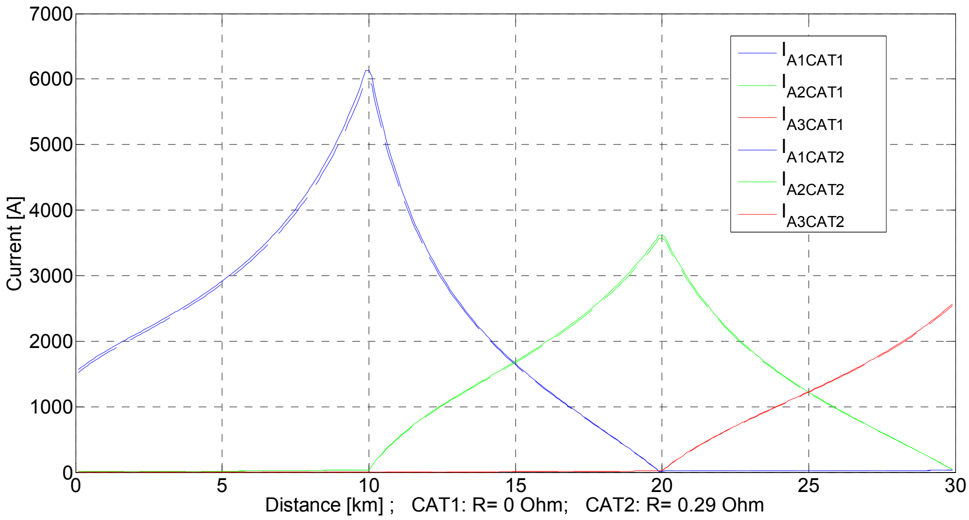

Figure 19. Simulated currents of the autotransformers AT1, AT2, and SATS for different fault locations. Fault between feeder and rail. Cases: (1) CAT1—no fault resistance, (2) CAT2—fault resistance of 0.29 Ω.

5. Experimental Tests

For the computer simulations, numerous experimental tests have been conducted in the laboratory to verify the influence of train circulation and arc resistance. A simplified diagram of the experimental setup is presented in Figure 20.

The experimental setup is displayed in Figure 21. It simulates the circuit of Figure 20. In the setup, the substation was executed by a power source (1) and the two winding traction transformers were implemented by two transformers, (2) and (3), providing 25 V_{AC} each. This implies a 1000-fold voltage reduction compared to the real 2 × 25 kV power system. The section comprised three subsections divided by the autotransformers ATS 1, ATS 2, and SATS (4). The impedances of the feeder and catenary were executed by inductive impedances Z (5). The ratings of these impedances (Z) were 0.5 + j5 Ω. Furthermore, the rail impedance was considered insignificant, therefore no impedance was connected. To perform ground faults along each subsection, variable impedances Z1 and Z2 (6) were employed. These variable inductances had 0.5 + j5 Ω each, with 10 taps available. So, the impedance per km was 0.1 + j1 Ω/km. Finally, to represent the trains and arc resistances, some adjustable resistors were used (7). The values of the impedance were similar to the values in the 2 × 25 kV power systems.

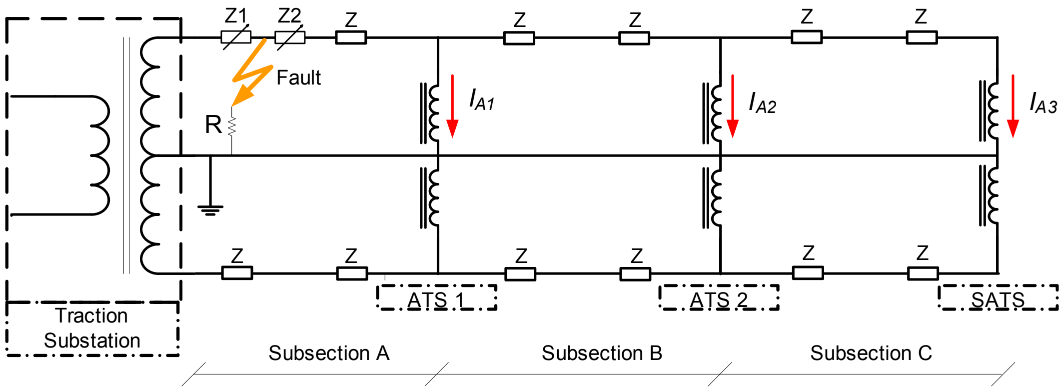

Figure 20. Simplified diagram of laboratory setup for ground fault testing of a 2 × 25 kV power system.

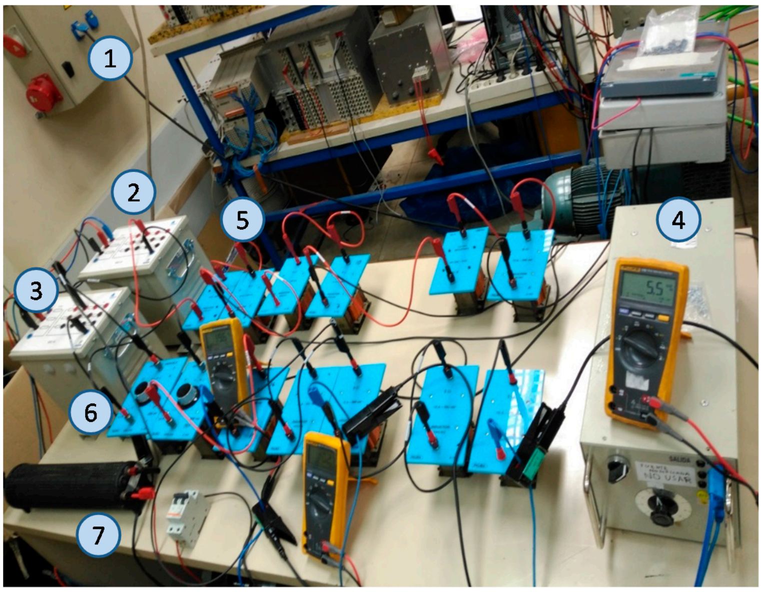

Figure 21. Laboratory setup for ground fault testing of a 2 × 25 kV power system.

As the values of the voltages were 1000 times smaller and the values of the impedances were similar to the values in the 2 × 25 kV power system, the currents measured in the experimental setup are 1000 times smaller. In other words, a volt represents a kilovolt and an amp represents a kiloampere.

The currents I_{A1}, I_{A2}, and I_{A3} were measured in the experimental setup. The currents were flowing through the autotransformers in the case of ground faults between rail and catenary and between rail and feeder. The ground faults were performed along a section simulating a 30-km length. The ground faults were performed every 0.5 km.

5.1. Experimental Tests on Influence of Train Power Consumption

The laboratory tests to analyse the effect of train circulation on the current values in the autotransformers and therefore on the ground fault location method were performed according to the circuit shown in Figure 22.

The high-speed train consumption was represented by a 50 Ω resistance. The current through this resistance was equivalent to the current of a high-speed train consuming 12.50 MW. This resistance

R was connected between catenary and rail in different positions; for example, in Figure 21, it was placed in the midpoint of section B.

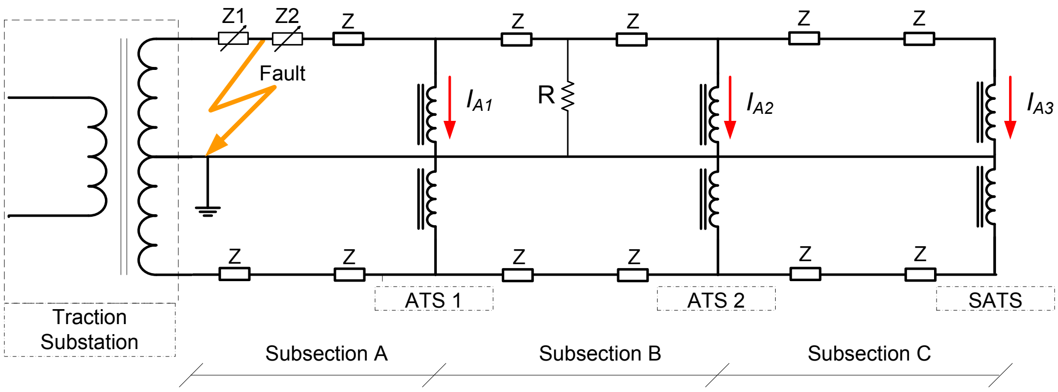

Figure 22. Laboratory setup for ground fault testing of a 2 × 25 kV power system with a high-speed train in the midpoint of section B simulated by resistance.

The results of the experimental tests are presented in Figures 23 and 24 for catenary and feeder ground faults, respectively.

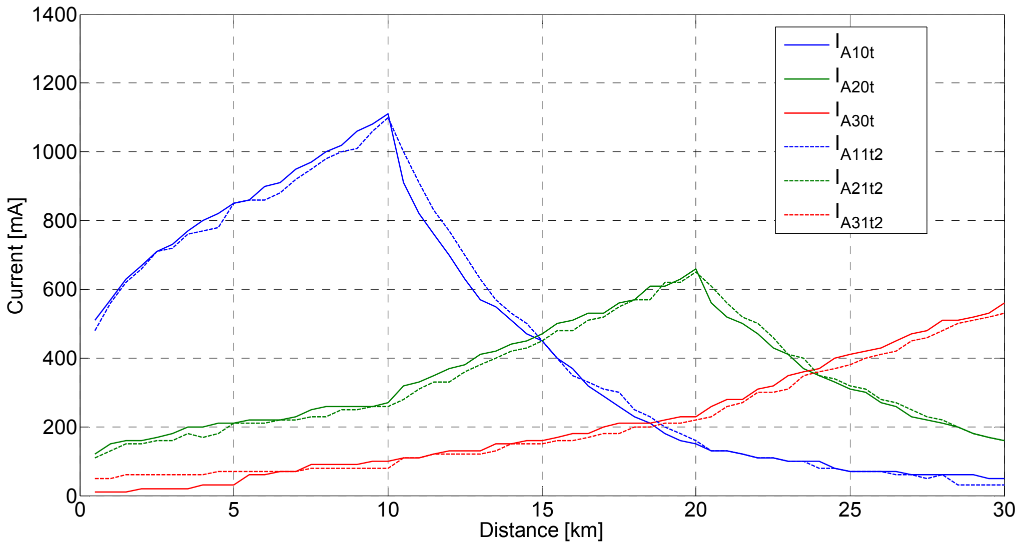

Figure 23. Autotransformer current distribution in the tests with a fault between the catenary and rail. Cases: (**a**) no trains (I_{Ai0t}), (**b**) one train in the midpoint of subsection B (I_{Ai1t2}).

In Figure 23, the current modules of the autotransformers I_{A1}, I_{A2}, and I_{A3} are represented for different catenary ground faults along the 30-km section with a train in the midpoint of subsection B (1*t*2). In addition, tests without high-speed trains are included (*0t*) to be able to make a comparison.

In Figure 24, the current modules of the autotransformers I_{A1}, I_{A2}, and I_{A3} are represented for different feeder ground faults along the 30-km section.

In this figure, the cases of a train in the midpoint of subsection C (I_{Ai1t3}) and two trains in the midpoint of subsections A and C ($I_{Ai2t1y3}$) are presented. In addition, tests without high-speed trains are included (0*t*) in order to compare the results.

It is clearly observed from the results presented in Figures 23 and 24 that the influence of the trains on the autotransformer currents is irrelevant, even in the case of two trains running in the same section simultaneously. Also, the experimental results are similar to the simulation results testing the reliability of this ground fault location method.

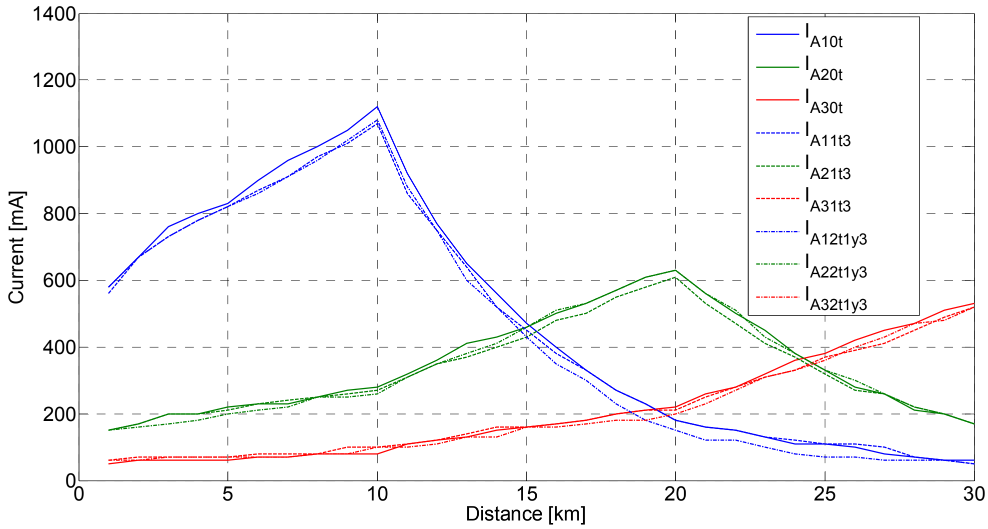

Figure 24. Autotransformer current distribution in the tests with a fault between the feeder and rail. Cases: (**a**) no trains (I_{Ai0t}), (**b**) one train in the midpoint of subsection C (I_{Ai1t3}), (**c**) two trains in the midpoint of subsection A and C ($I_{Ai2t1y3}$).

5.2. Laboratory Tests of Influence of Fault Resistance

In order to study the influence of the fault resistance, the circuit presented in Figure 25 was used. A fault resistance (R) of 0.30 Ω was installed between catenary and ground or feeder and ground depending on the test.

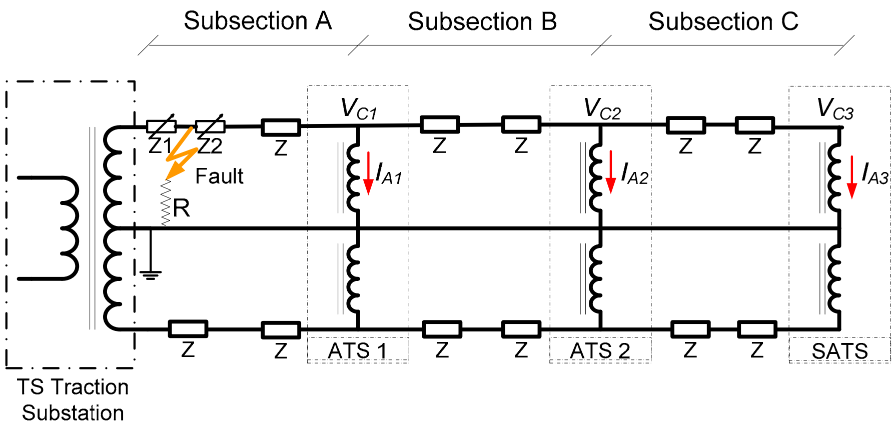

Figure 25. Laboratory setup for ground fault testing of a 2 × 25 kV power system with fault resistances.

The results of the experimental tests are presented in Figures 26 and 27 for catenary and feeder ground faults, respectively.

In Figures 26 and 27, the current modules of the autotransformers I_{A1}, I_{A2}, and I_{A3} are represented for catenary and feeder ground faults, respectively, along the 30-km section. In these tests, different fault resistances of 0 and 0.30 Ω have been used.

It can be observed from the results presented in Figures 26 and 27 that the experimental results are similar to the results of simulations. We can conclude that the influence of the fault resistance on the autotransformer currents is insignificant.

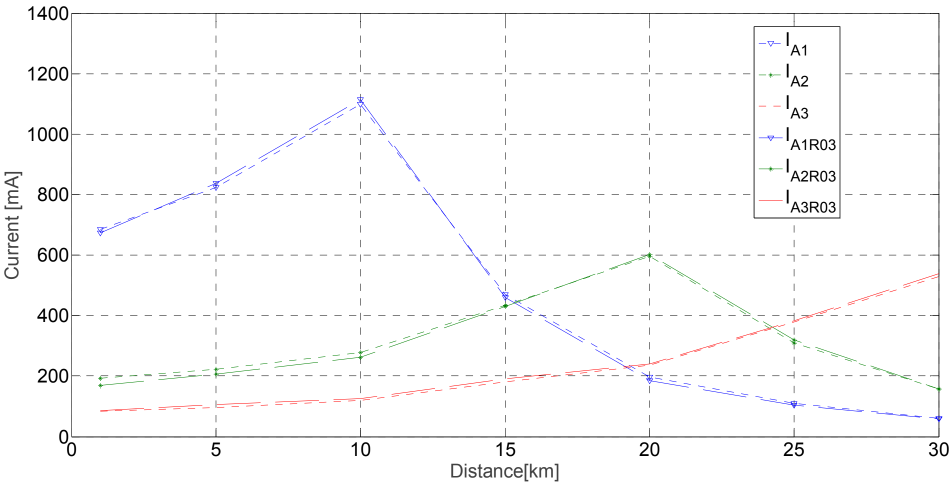

Figure 26. Autotransformer current distribution in the tests with a fault between the catenary and rail with fault resistances of: (**a**) 0 Ω and (**b**) 0.3 Ω.

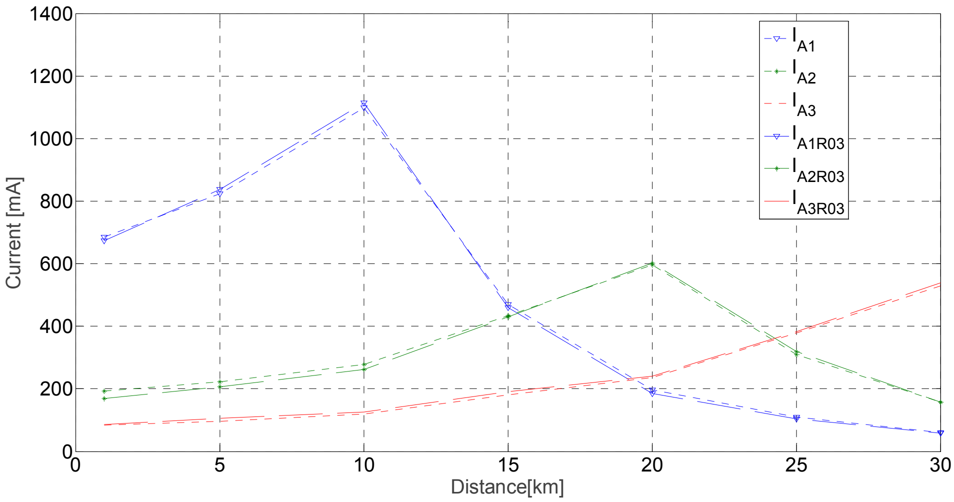

Figure 27. Autotransformer current distribution in the tests with a fault between the feeder and rail with fault resistances of (**a**) 0 Ω and (**b**) 0.3 Ω.

5.3. Validation of the Experimental Setup by Simulations

In order to verify the experimental setup, we have developed a simulation model with the impedances used (Table 2). The results of the simulations (Figure 28) are very close to the experimental results (Figures 23, 24 and 26).

Table 2. Self-impedance values of the railway conductors.

Conductor		**Impedance (Ω/km)**
Catenary	Z_C	0.100 + j1.000
Feeder	Z_F	0.100 + j1.000
Rail	Z_R	0

The short-circuit current distributions results obtained in the experimental setup and in the simulations are similar to the results presented in [19]. This reference is one of the most prestigious references of short-circuit current calculation in 2 × 25 kV power systems.

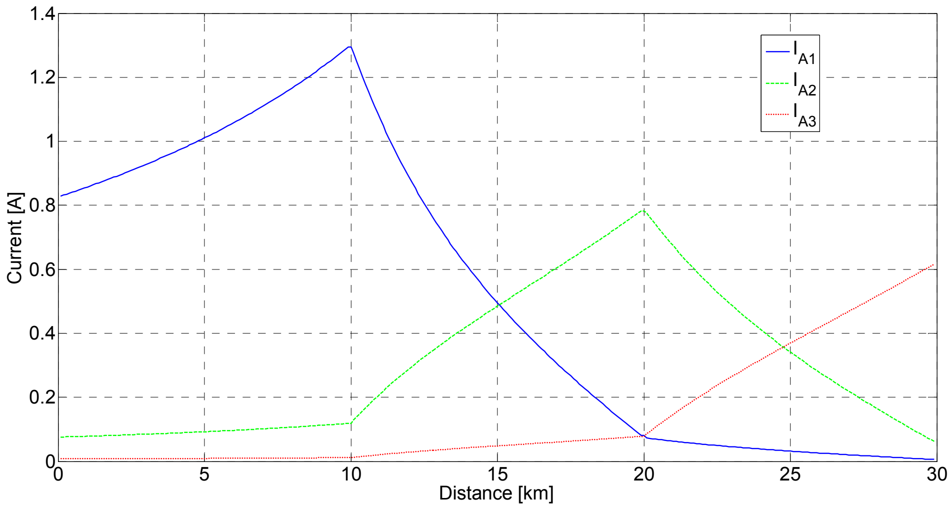

Figure 28. Currents obtained in simulations of the autotransformers AT1, AT2, and SATS of the experimental model.

6. Conclusions

In this paper, the influence of train circulation and arc resistance on a novel method of ground fault location for 2 × 25 kV traction power systems has been studied. The location system is based on the measurement of the voltages and currents in the autotransformers and compared to the previous theoretically calculated values. Previously, the analysis of the phase angle between the voltages and the currents in the autotransformers defines the subsection and the conductor, catenary or feeder, where the ground fault takes place.

As train circulation and fault resistances modify the theoretically calculated current values in the autotransformers, these factors could produce errors in the location of the ground faults.

These influences have been studied by computer simulations and experimental tests in the laboratory.

After numerous simulations, the maximum error in fault current does not reach 5%.

On the other hand, in the experimental tests, the maximum error in fault current does not reach 6%.

The main conclusion of this paper is that the location method is not significantly influenced by train circulation and arc fault resistances, so the use of this method facilitates the location of the ground fault.

Author Contributions: C.A.P. performed the laboratory tests and wrote the manuscript. J.S. developed the simulation models and reviewed the manuscript. M.L.-T. revised and improved the simulation model. R.G. analyzed the results and checked the manuscript.

Funding: This research received no external funding.

Conflicts of Interest: The authors declare no conflict of interest.

Abbreviations

The following abbreviations are used in this manuscript:

AC:	Alternating current
AT:	Autotransformer
ATS:	Autotransformer station
I:	Fault current
I_{A1}:	Catenary current in autotransformer 1
I_{A2}:	Catenary current in autotransformer 2
I_{A3}:	Catenary current in autotransformer 3
i:	Autotransformer number: 1, 2, 3, . . . , N

I_{Ai}: Current input from catenary in autotransformer "i"
L: Arc length
R Arc resistance
SATS: Autotransformer station at the end of the section
$V1$: Voltage source 1
$V2$: Voltage source 2
V_{Ci}: Catenary voltage in autotransformer "i"
Z: Experimental setup inductive impedance
Z1: Experimental setup adjustable inductive impedance 1
Z2: Experimental setup adjustable inductive impedance 2
Z_C: Catenary self-impedance value per unit length
Z_F: Feeder self-impedance value per unit length
Z_R: Rail self-impedance value per unit length
Z_{CF}: Mutual impedance catenary–feeder value per unit length
Z_{CR}: Mutual impedance catenary–rail value per unit length
Z_{FR}: Mutual impedance feeder–rail value per unit length

References

1. Hill, R.J. Electric Railway Traction. Part 3. Traction Power Supplies. *Power Eng. J.* **1994**, *8*, 275–286. [CrossRef]
2. Mariscotti, A.; Pozzobon, P.; Vanti, M. Distribution of the Traction Return Current in AT Electric Railway Systems. *IEEE Trans. Power Deliv.* **2005**, *20*, 2119–2128. [CrossRef]
3. Areva T&D. *Network Protection & Automation Guide*; Areva T&D Energy Automation & Information: Levallois-Peret, France, 2002; Volume 20, pp. 353–369.
4. Zhou, Y.; Xu, G.; Chen, Y. Fault Location in Power Electrical Traction Line System. *Energies* **2012**, *5*, 5002–5018. [CrossRef]
5. Lin, G.S.; Li, Q.Z. Impedance Calculations for AT Power Traction Networks with Parallel Connections. In Proceedings of the 2010 Asia-Pacific Power and Energy Engineering Conference, Chengdu, China, 28–31 March 2010; pp. 1–5.
6. Agarwal, K.K. Automatic Fault Location and Isolation System for the Electric Traction Overhead Lines. In Proceedings of the 2002 ASME/IEEE Joint Railroad Conference, Washington, DC, USA, 23–25 April 2002; pp. 117–122.
7. Hewings, D.B.; Chen, J.; Storey, A.P. Application of a New Distance Protection Scheme to a Single-Pole Autotransformer Electrification System on the UK West Coast Main Line Railway. In Proceedings of the IET 9th International Conference on Developments in Power System Protection, Glasgow, Scotland, UK, 17–20 March 2008; pp. 56–61.
8. Fujie, H.; Miura, A. Fault Location System in Autotransformer Feeding Circuit of AC Electric Railways. *Electr. Eng. Jpn.* **1976**, *5*, 96–105. [CrossRef]
9. Wang, C.; Yin, X. Comprehensive Revisions on Fault-Location Algorithm Suitable for Dedicated Passenger Line of High-Speed Electrified Railway. *IEEE Trans. Power Deliv.* **2012**, *27*, 2415–2417. [CrossRef]
10. Lee, H.; Oh, S.; Kim, G.; An, C. A Study on the Equivalent Conductor Representation of AC Electric Railway System. In Proceedings of the 2009 International Conference on Information and Multimedia Technology, Jeju Island, South Korea, 16–18 December 2009; pp. 33–37.
11. Wang, X.; Qian, Q.; Chen, W. Analyzing Fault-Induced Transients with Wavelets. In Proceedings of the IEEE Power Engineering Society Summer Meeting, Chicago, IL, USA, 21–25 July 2002; pp. 1090–1093.
12. Zhang, D.; Wu, M.; Xia, M. Study on Traveling Wave Fault Location Device for Electric Railway Catenary System Based on DSP. In Proceedings of the International Conference on Sustainable Power Generation and Supply, Nanjing, China, 6–7 April 2009; pp. 1–4.
13. Xu, G.; Zhou, Y.; Chen, Y. Model-Based Fault Location with Frequency Domain for Power Traction System. *Energies* **2013**, *6*, 3097–3114. [CrossRef]
14. Battistelli, L.; Pagano, M.; Proto, D. Short Circuit Modelling and Simulation of 2 × 25 kV High Speed Railways. In Proceedings of the Second Asia International Conference on Modelling & Simulation (AMS), Kuala Lumpur, Malaysia, 13–15 May 2008; pp. 702–707.

15. Serrano, J.; Platero, C.A.; López-Toledo, M.; Granizo, R. A Novel Ground Fault Identification Method for 2×25 kV Railway Power Supply Systems. *Energies* **2015**, *8*, 7020–7039. [CrossRef]
16. Serrano, J.; Platero, C.A.; López-Toledo, M.; Granizo, R. A New Method of Ground Fault Location in 2×25 kV Railway Power Supply Systems. *Energies* **2017**, *10*, 340. [CrossRef]
17. Andrade, V.; Sorrentino, E. Typical Expected Values of the Fault Resistance in Power Systems. In Proceedings of the IEEE/PES Transmission and Distribution Conference and Exposition: Latin America (T&D-LA), Sao Paulo, Brazil, 8–10 November 2010; pp. 602–609.
18. Wedepohl, L.M.; Jackson, L. Modified nodal analysis: An essential addition to electrical circuit theory and analysis. *Eng. Sci. Educ. J.* **2002**, *11*, 84–92. [CrossRef]
19. Chen, T.-H.; Hsu, Y.-F. Systematized short-circuit analysis of a 2×25 kV electric traction network. *Electr. Power Syst. Res.* **1998**, *47*, 133–142. [CrossRef]